Nanoscale Res Lett (2009) 4:221–228
DOI 10.1007/s11671-008-9229-y

NANO EXPRESS

Magnesium Ferrite ($MgFe_2O_4$) Nanostructures Fabricated by Electrospinning

Santi Maensiri · Montana Sangmanee · Amporn Wiengmoon

Received: 14 August 2008 / Accepted: 2 December 2008 / Published online: 16 December 2008

Abstract Magnesium ferrite ($MgFe_2O_4$) nanostructures were successfully fabricated by electrospinning method. X-ray diffraction, FT-IR, scanning electron microscopy, and transmission electron microscopy revealed that calcination of the as-spun $MgFe_2O_4$/poly(vinyl pyrrolidone) (PVP) composite nanofibers at 500–800 °C in air for 2 h resulted in well-developed spinel $MgFe_2O_4$ nanostuctures. The crystal structure and morphology of the nanofibers were influenced by the calcination temperature. Crystallite size of the nanoparticles contained in nanofibers increased from 15 ± 4 to 24 ± 3 nm when calcination temperature was increased from 500 to 800 °C. Room temperature magnetization results showed a ferromagnetic behavior of the calcined $MgFe_2O_4$/PVP composite nanofibers, having their specific saturation magnetization (M_s) values of 17.0, 20.7, 25.7, and 31.1 emu/g at 10 Oe for the samples calcined at 500, 600, 700, and 800 °C, respectively. It is found that the increase in the tendency of M_s is consistent with the enhancement of crystallinity, and the values of M_s for the $MgFe_2O_4$ samples were observed to increase with increasing crystallite size.

S. Maensiri · M. Sangmanee
Department of Physics, Faculty of Science, Small & Strong Materials Group (SSMG), Khon Kaen University, Khon Kaen 40002, Thailand

S. Maensiri (✉) · M. Sangmanee
Integrated Nanotechnology Research Center (INRC), Faculty of Science, Khon Kaen University, Khon Kaen 40002, Thailand
e-mail: sanmae@kku.ac.th; santimaensiri@gmail.com

A. Wiengmoon
Department of Physics, Faculty of Science, Naresuan University, Phitsanulok 65000, Thailand

Keywords Magnesium ferrite · Nanofibers · Electrospinning · Electron microscopy · X-ray diffraction · Magnetic properties · Nanofabrication

Introduction

Spinel ferrites with the general formula AFe_2O_4 (A = Mn, Co, Ni, Mg, or Zn) are very important magnetic materials because of their interesting magnetic and electrical properties with chemical and thermal stabilities [1]. Magnesium ferrite ($MgFe_2O_4$) is one of the most important ferrites. It has a cubic structure of normal spinel-type and is a soft magnetic *n*-type semiconducting material, which finds a number of applications in heterogeneous catalysis, adsorption, sensors, and in magnetic technologies [2]. Recently, nanostructures of magnetic materials have received more and more attention due to their novel material properties that are significantly different from those of their bulk counterparts [3–7]. The ordered magnetic materials such as nanorods and nanowires have currently attracted a great interest due to their enhanced magnetic property [8, 9]. So far, reported nanostructures $MgFe_2O_4$ are mostly in the form of nanoparticle [10–22], whereas other nanostructured forms of $MgFe_2O_4$ have not been reported. Large surface-to-volume ratio is an attractive characteristic that can be achieved from nanofiberization of magnetic materials. With such feature, their technological application should be expressed into many areas including nanocomposites, nanocatalysts, nanosensors, nano-electronics, and photonics.

A number of methods have been developed to fabricate materials with nanofibrous structures, including an electrospinning which is a simple and convenient method for preparing polymer fibers and ceramic fibers with both solid

and hollow interiors that are exceptionally long in length, uniform in diameter ranging from tens of nanometers to several micrometers, and diversified in compositions [23, 24]. In an electrospinning process [25], an electrical potential is applied between a droplet of a polymer solution held at the end of the nozzle of the spinneret and a ground target. When the applied electric field overcomes the surface tension of the droplet, a charged jet of polymer solution is ejected. The route of the charged jet is controlled by the electric field. The jet exhibits bending instabilities caused by repulsive forces between the charges carried with the jet. The jet extends through spiralling loops. As the loops increase in diameter the jet grows longer and thinner until it solidifies or is collected on the target.

To date, electrospun ferrite nanofibers of $NiFe_2O_4$ [26], $CoFe_2O_4$ [27], $MnFe_2O_4$ [28], and $CuFe_2O_4$ [29] have been reported. To the best of our knowledge, electrospinning of $MgFe_2O_4$ has not yet been reported. Thus, the present work investigated the fabrication of $MgFe_2O_4$ nanofibers by electrospinning using a solution that contained poly(vinyl pyrrolidone) (PVP) and cheap Mg and Fe nitrates as metal sources. The samples of as-spun and calcined $MgFe_2O_4$/PVP composite were characterized by thermogravimetric-differential thermal analysis (TG-DTA), X-ray diffraction (XRD), FT-IR, scanning electron microscopy (SEM), and transmission electron microscopy (TEM). The magnetic properties of calcined $MgFe_2O_4$/PVP composite samples were investigated using a vibrating sample magnetometer (VSM) at room temperature. The effects of calcination temperature on morphology, structure, and magnetic properties of the fabricated samples were also studied.

Experimental Section

In this study, $Mg(NO_3)_2 \cdot 6H_2O$ (99% purity, Kanto Chemicals, Japan), $Fe(NO_3)_3 \cdot 9H_2O$ (99.99% purity, Kanto Chemicals, Japan) and PVP ($M_n = 1{,}300{,}000$, Aldrich), *N*,*N*-Dimetylformamide (DMF) (99.8% purity, Fluka, Switzerland), acetic acid (100% purity, BDH, England), and ethanol (100% purity, BDH, England) were used as the starting chemicals. In the preparation of the solution for electrospinning, we used a solution that contained PVP mixed with $Mg(NO_3)_2 \cdot 6H_2O$ and $Fe(NO_3)_3 \cdot 9H_2O$. A PVP/ethanol solution was prepared using a ratio of 1.0 g PVP to 9 mL ethanol. A metal nitrates/DMF solution was prepared by dissolving 0.01 mol $Mg(NO_3)_2 6H_2O$ and 0.02 mol $Fe(NO_3)_3 \cdot 9H_2O$ in 10 mL of DMF and stirred for 5 h. Subsequently, the metal nitrates/DMF solution (4 mL) was added slowly to the PVP/ethanol solution (50 mL) under vigorous stir at 27 °C for 5 h to obtain a well-dissolved solution. This final solution was used for electrospinning.

The prepared polymer solution was loaded into a plastic syringe equipped with a 22-gauge needle made of stainless steel. The electrospinning process was carried out using our home-made electrospinning system. The electrospinning system and schematic diagram of electrospinning process are shown in Fig. 1. The needle was connected to a high-voltage supply and for each solution the voltage of 15 kV was applied. The solution was fed at a rate of 0.5 mL/h using a motor syringe pump. A piece of flat aluminum foil was placed 15 cm below the tip of the needle, and used to collect the nanofibers. All electrospinning processes were carried out at room temperature.

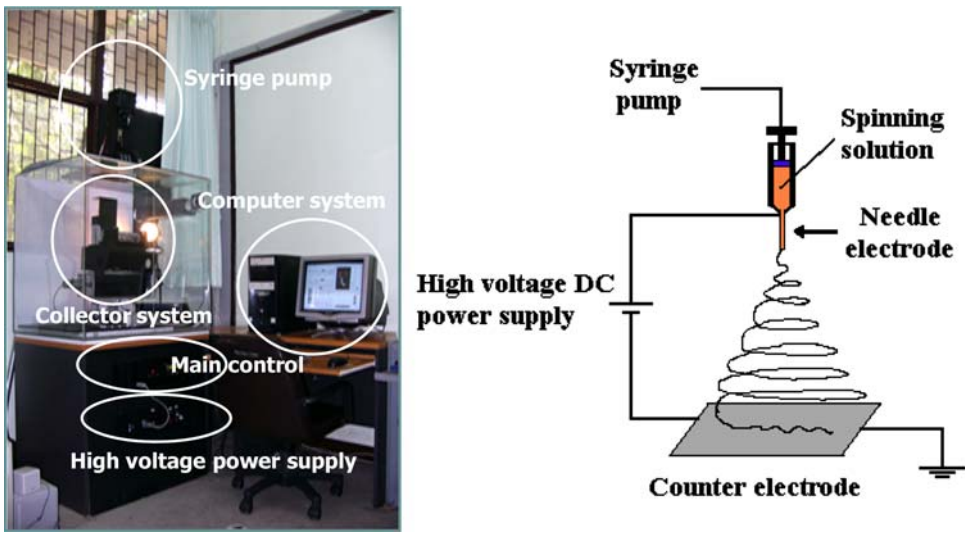

Fig. 1 An electrospinning system (left) and schematic diagram of electrospinning set up (right)

The as-spun $MgFe_2O_4$/PVP composite nanofibers were subjected to TG-DTA using Pyris Diamond TG/DTA (PerkinElmer Instrument, USA). This was done to determine the temperatures of possible decomposition and crystallization (or phase changes) of the as-spun nanofibers. The analyses were performed with a heating rate of 5 °C/min in static air up to 1000 °C. The composite nanofibers were calcined at 500, 600, 700, and 800 °C for 2 h in air in box furnace (Lenton Furnaces, UK), using heating and cooling rates of 5 °C/min. The final products obtained were brown $MgFe_2O_4$ samples. The as-spun and calcined composite nanofibers were characterized by means of XRD using Cu*K*a radiation with $\lambda = 0.15418$ nm (PW3040 mpd control, The Netherlands), FT-IR spectroscopy (Spectrum One FT-IR Spectrometer, PerkinElmer Instruments, USA), SEM (Hitachi FE-SEM S–4700, Japan), and TEM (Philips Tecnai 12 G2 TEM, at 120 kV, The Netherlands). The average diameters of the as-spun and calcined composite nanofibers were determined from about 300 measurements. The magnetic properties of the calcined samples were examined at room temperature (20 °C) using a VSM (Lake Shore VSM 7403, USA).

Results and Discussion

The TG curve in Fig. 2 shows a minor weight loss step (~20%) from 30 up to about 270 °C and two major weight loss steps from 270 to 455 °C (~60%). No further weight loss was observed up to 1000 °C. The minor weight loss was related to the loss of moisture and trapped solvent (water, ethanol, and carbon dioxide) in the as-spun $MgFe_2O_4$/PVP composite nanofibers, whereas the major weight loss was due to the combustion of organic PVP matrix. On the DTA curve, main exothermic peaks were observed at ~290 and ~450 °C, suggesting the thermal

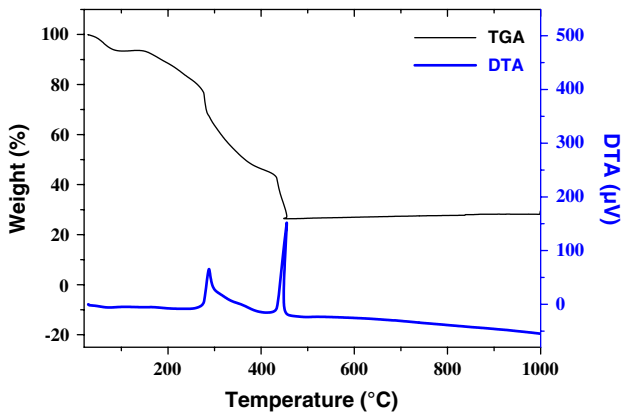

Fig. 2 TG-DTA curves of thermal decomposition of the as-spun $MgFe_2O_4$/PVP composite nanofibers at a heating rate of 5 °C/min in static air

events related to the decomposition of Mg and Fe nitrates along with the degradation of PVP by dehydration on the polymer side chain, which was confirmed by a dramatic weight loss in TG curve at the corresponding temperature range (270–455 °C). The plateau formed between 455 and 1000 °C on the TG curve indicated the formation of crystalline $MgFe_2O_4$ as the decomposition product [30, 31], as confirmed by XRD and FT-IR analyses as shown in Figs. 6 and 7, respectively.

The morphology of the as-spun and calcined $MgFe_2O_4$/PVP composite nanofibers was revealed by SEM. Figure 3 shows the SEM micrographs and the respective diameter histogram of the as-spun $MgFe_2O_4$/PVP composite nanofibers. The as-spun composite nanofibers appeared quite smooth due to the amorphous nature of $MgFe_2O_4$/PVP composite. Each individual nanofiber was quite uniform in cross section, and the average diameter of the fibers was 134 ± 35 nm. The PVP was selectively removed by calcination of the as-spun composite nanofibers in air at 500, 600, 700, and 800 °C. Figure 4 shows the SEM micrographs of the calcined $MgFe_2O_4$/PVP composite nanofibers. All the calcined nanofibers formed a structure of packed particles or crystallites. These changes in the morphology are related to a dramatic change in crystal structure as observed in electrospun $NaCo_2O_4$ [30], $Ba_{0.6}Sr_{0.4}TiO_3$ [31], and TiO_2 [32]. The nanofibers calcined at 500 °C remained as continuous structures (Fig. 4a), having fiber size of ~100 nm in diameter. The reduction in size of the nanofibers should be attributed to the loss of PVP from the nanofibers and the crystallization of $MgFe_2O_4$. After calcination above 500 °C, the nature of nanofibers was changed, and a structure of packed particles or crystallites was prominent, which may be due to the reorganization of the $MgFe_2O_4$ structure at high temperature. From Fig. 4, the particle sizes of the calcined samples of $MgFe_2O_4$/PVP composite nanofibers are <50 nm.

The detailed morphology and crystalline structure of the $MgFe_2O_4$/PVP composite nanofibers calcined at 700 and 800 °C for 2 h were further investigated by TEM, and the TEM bright-field images with corresponding selected-area electron diffraction (SAED) patterns of these two samples are shown in Fig. 5. It is clearly seen from the TEM bright-field images that both samples consisted of packed $MgFe_2O_4$ particles or crystallites with particle sizes of ~10–20 and 25–80 nm in diameter for the samples of 700 °C-calcined and 800 °C-calcined composite nanofibers, respectively. It is seen that the particle sizes of $MgFe_2O_4$ contained in the calcined $MgFe_2O_4$/PVP composite nanofibers are quite uniform. This might have resulted from the rates of hydrolysis involved in the fabrication process in which the water required for the hydrolysis of metal precursors was supplied by the moisture in air [26]. Since the electrospun fibers were very

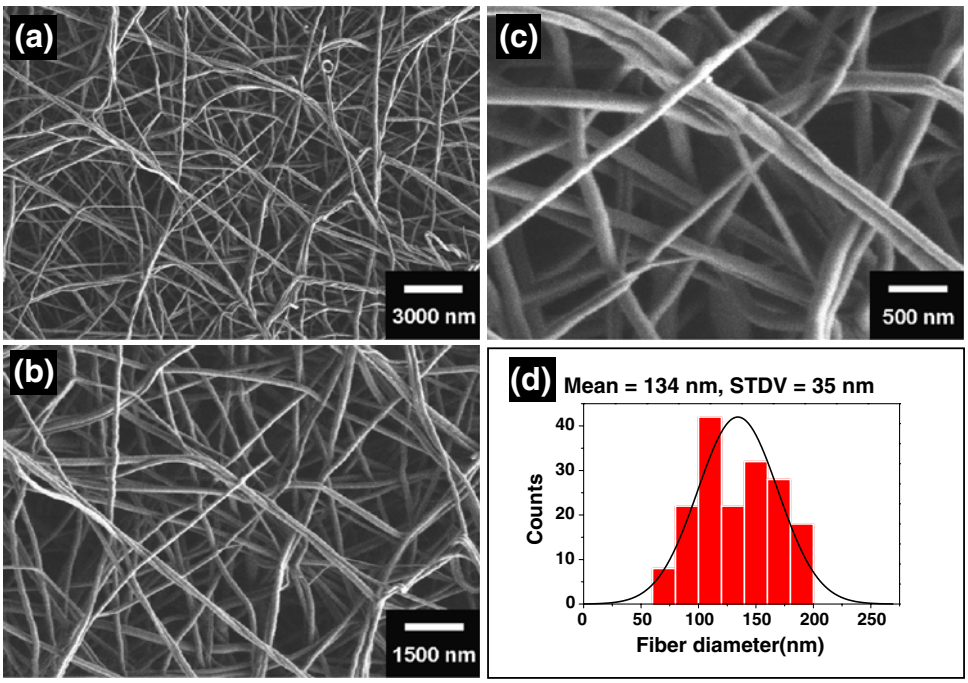

Fig. 3 SEM micrographs and fiber size distribution histogram of the as-spun $MgFe_2O_4$/PVP composite sample a. **a** 5,000× SEM image, **b** 10,000× SEM image, **c** 30,000× SEM image, and **d** fiber size distribution histogram

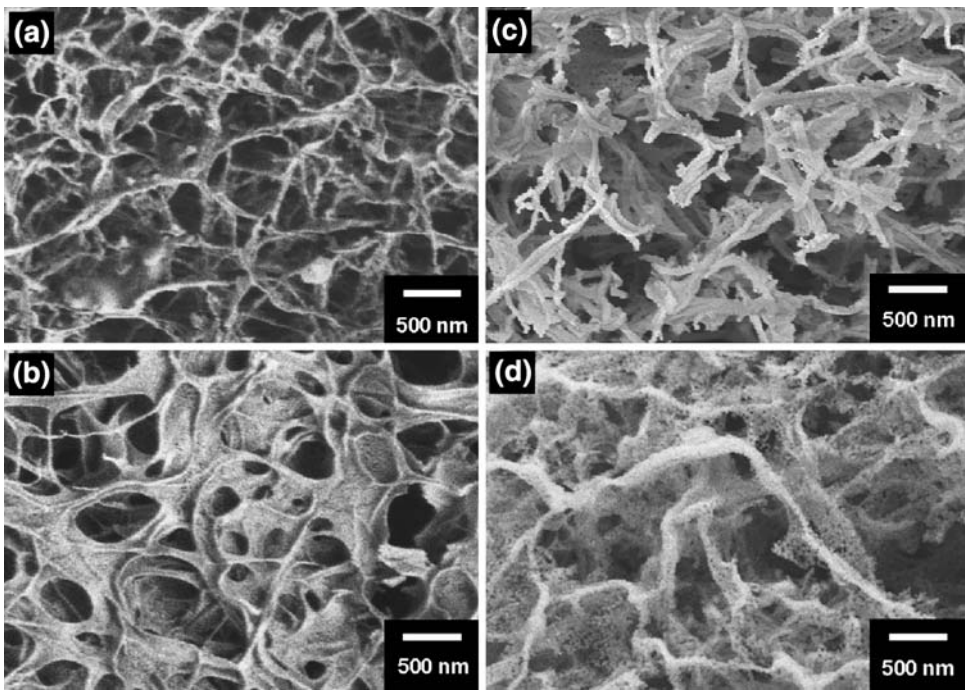

Fig. 4 SEM micrographs of the $MgFe_2O_4$/PVP composite samples calcined in air at different temperatures for 2 h. **a** 500 °C, **b** 600 °C, **c** 700 °C, and **d** 800 °C

small in diameter, the moisture could quickly diffuse into the fibers, causing a rapid and uniform hydrolysis of the metal precursors. The corresponding SAED patterns (Fig. 5) of both samples show spotty ring patterns without any additional diffraction spots and rings of second phases, revealing their crystalline spinel structure. Measured interplanar spacings (d_{hkl}) from SAED patterns shown in Fig. 5 are in good agreement with the values in the standard data (JCPDS: 88-1935). The diffraction rings are identified as the (111), (220), (311), (400), (422), (511), and (440) planes. This concurs with the results of XRD presented in Fig. 6.

The XRD patterns of the calcined $MgFe_2O_4$/PVP composite nanofibers are shown in Fig. 6. All of the main peaks are indexed as the spinel $MgFe_2O_4$ in the standard data (JCPD no.: 8-1935). The average crystallite sizes of

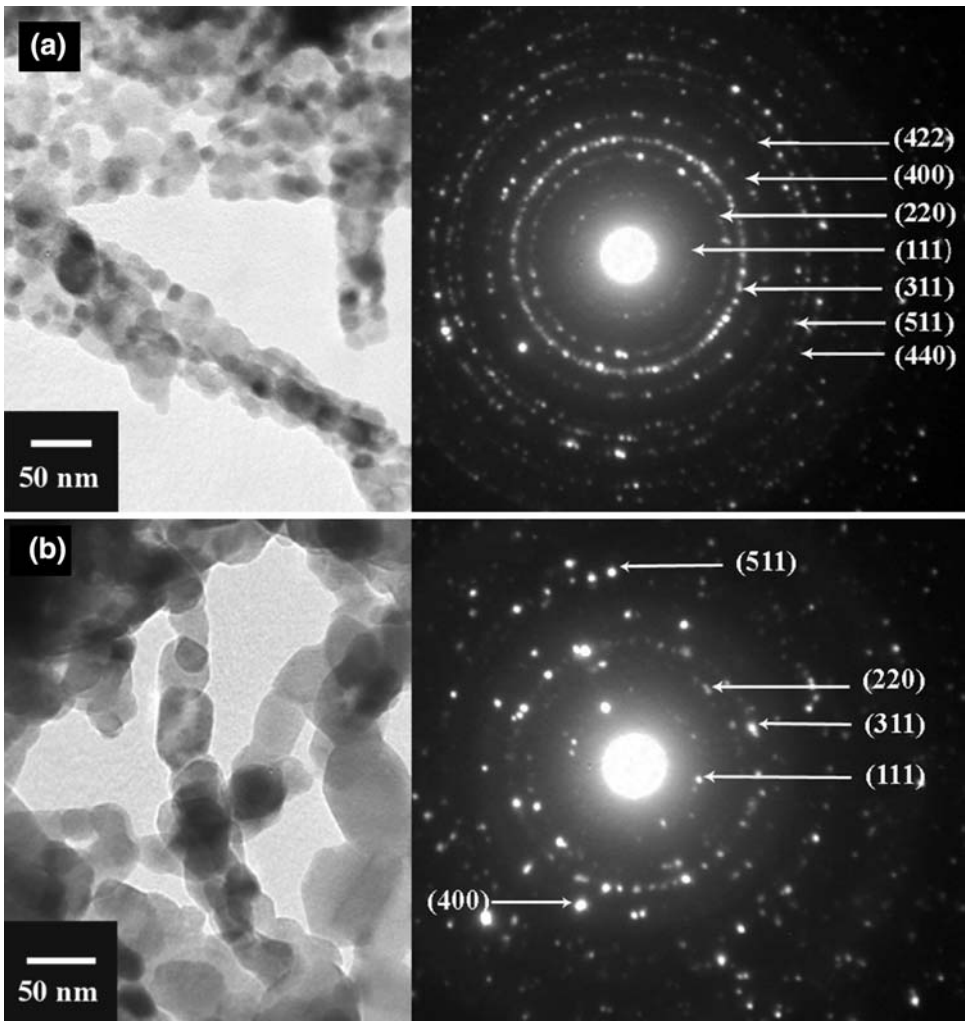

Fig. 5 TEM images with corresponding SAED patterns of the $MgFe_2O_4$/PVP composite samples calcined in air for 2 h at **a** 700 °C and **b** 800 °C

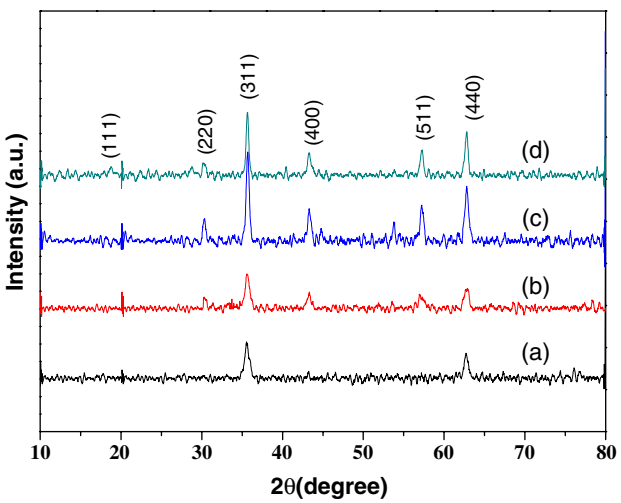

Fig. 6 XRD patterns of the $MgFe_2O_4$/PVP composite samples calcined in air for 2 h at different temperatures. **a** 500 °C, **b** 600 °C, **c** 700 °C, and **d** 800 °C

$CuFe_2O_4$ samples were calculated from X-ray line broadening of the reflections of (220), (311), (400), (511), and (440) using Scherrer's equation (i.e., $D = 0.89\lambda/(\beta \cos\theta)$, where λ is the wavelength of the X-ray radiation, K is a constant taken as 0.89, θ the diffraction angle, and β is the full width at half-maximum [33]), and were found to be 15 ± 4, 17 ± 1, 23 ± 2, and 24 ± 3 nm for the samples of $MgFe_2O_4$/PVP composite nanofibers calcined at 500, 600, 700, and 800 °C, respectively. The values of lattice parameter a calculated from the XRD spectra were 0.8372 ± 0.0007, 0.8362 ± 0.0012, 0.8353 ± 0.0011, and 0.8346 ± 0.0030 nm for the samples of $MgFe_2O_4$/PVP composite nanofibers calcined at 500, 600, 700, and 800 °C, respectively. The crystallite sizes and lattice parameters are also summarized in Table 1.

The formation of spinel $MgFe_2O_4$ structure in the calcined $MgFe_2O_4$/PVP composite nanofibers was further supported by FT-IR spectra (Fig. 7). Here, we consider two

Table 1 Average crystal sizes from XRD, spinel lattice parameter a calculated from XRD spectra, the specific magnetization (M_s), remnant magnetization (M_r), the ratio of the ratio of remnant magnetization to bulk saturation magnetization (M_r/M_s), and coercive forces (H_c) of the $MgFe_2O_4$/PVP composite samples calcined in air at 500, 600, 700, and 800 °C for 2 h

$MgFe_2O_4$ sample	Average crystallite size from XRD (nm)	Spinel lattice parameters a (nm)	M_s at 10 kOe (emu/g)	M_r (emu/g)	M_r/M_s	H_c (Oe)
Calcined at 500 °C	15 ± 4	0.8372 ± 0.0007	17.0	0.6	0.035	35.8
Calcined at 600 °C	17 ± 1	0.8362 ± 0.0012	20.7	0.8	0.040	37.6
Calcined at 700 °C	23 ± 2	0.8353 ± 0.0011	25.7	2.4	0.095	71.2
Calcined at 800 °C	24 ± 3	0.8346 ± 0.0030	31.1	4.7	0.151	98.9

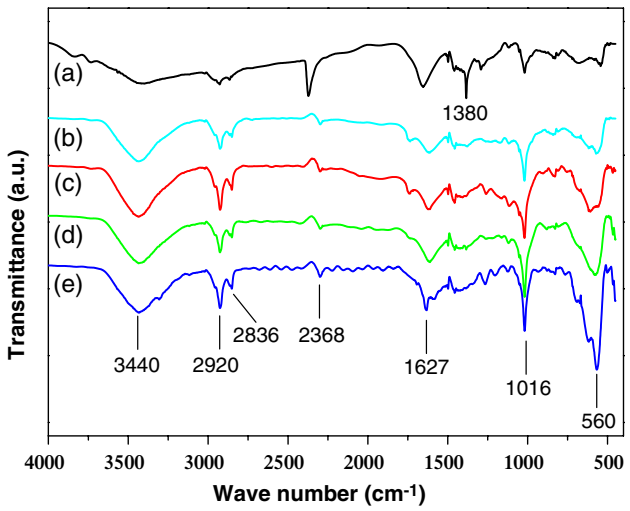

Fig. 7 FT-IR spectra of the $MgFe_2O_4$/PVP composite samples calcined in air for 2 h at different temperatures. **a** As-spun, **b** 500 °C, **c** 600 °C, **d** 700 °C, and **e** 800 °C

ranges of the absorption bands: 4000–1000 and 1000–400 cm^{-1} as suggested by previously published studies [13, 34]. In the range of 4000–1000 cm^{-1}, vibrations of CO_3^{2-} and moisture were observed. The intensive band at ~1627 cm^{-1} is due to O–H stretching vibration interacting through H bonds. The band at ~2920 cm^{-1} is C–H asymmetric stretching vibration mode due to the $–CH_2–$ groups of the long aliphatic alkyl groups. The ν(C=O) stretching vibration of the carboxylate group (CO_2^{2-}) was observed around 1380 cm^{-1} and the band at ~1016 cm^{-1} was corresponded to nitrate ion traces. Therefore the CO_3^{2-} and CO_3^{-} vibrations disappeared when calcination temperature was increased. In the range of 1000–400 cm^{-1}, a typical metal–oxygen absorption band for the spinel structure of the ferrite at ~560 cm^{-1} was observed in the FT-IR spectra of all of the calcined $MgFe_2O_4$ samples. This band strongly suggests the intrinsic stretching vibrations of the metal (Fe ↔ O) at the tetrahedral site [34–37].

The specific magnetization curves of the calcined $MgFe_2O_4$/PVP composite nanofibers obtained from room temperature VSM measurement are shown in Fig. 8. These curves are typical for a soft magnetic material and indicate hysteresis ferromagnetism in the field range of ±500 Oe, while outside this range the specific magnetization increases with increasing field and tends to saturate in the field range investigated (±10 kOe). The specific saturation magnetization (M_s) values of 17.0, 20.7, 25.7, and 31.1 emu/g at 10 kOe were observed for the $MgFe_2O_4$/PVP composite nanofibers calcined at 500, 600, 700, and 800 °C, respectively. It is found that the increase in the tendency of M_s is consistent with the enhancement of crystallinity, and the values of M_s for the $MgFe_2O_4$ samples were observed to increase with increasing crystallite size. This type of behavior is entirely consistent with a model of crystal growth in such a way that the difference in the magnetic parameters is associated with the change in crystallite size [38]. Noted that the saturation value of 31.1 emu/g obtained in the sample calcined at 800 °C (crystallite size of 24 ± 3 nm) is close to the values of 33.4 emu/g for bulk $MgFe_2O_4$ [18] and 30.6 emu/g for sol–gel/combustion synthesized $MgFe_2O_4$ (crystallite size of ~78 nm) [13], while it is higher than the values of ~14.09 emu/g for coprecipitation-synthesized $MgFe_2O_4$ nanoparticles (diameters of ~34.4 nm) [21] and 15.3 emu/g for sol–gel-derived $MgFe_2O_4$ nanoparticles (diameters of ~42 nm) [22].

From Fig. 8, the remnant magnetization (M_r) values of 0.6, 0.8, 2.4, and 4.7 emu/g were observed for the $MgFe_2O_4$/PVP composite nanofibers calcined at 500, 600, 700, and 800 °C, respectively. As a result, the ratio of remnant magnetization to bulk saturation magnetization, M_r/M_s, of the $MgFe_2O_4$/PVP composite nanofibers calcined at 500, 600, 700, and 800 °C was obtained to be 0.035, 0.040, 0.095, and 0.151, respectively. The low values of M_r/M_s indicate an appreciable fraction of superparamagnetic particles. The increase in M_r/M_s from 0.035 to 0.151 is consistent with results obtained on $MgFe_2O_4$ nanoparticles reported by Rashad [21], in which M_r/M_s was increased from 0.113 to 0.137 when particle size increased from 27.2 to 112 nm. However, our results and those of Ref. [21] are not consistent with results obtained on typical ferromagnetic particles reported in Ref. [39]. For ferromagnetic nanoparticles, it is interesting to note that the

magnetization is strongly dependent on their particle size, as shown by electron holographic study of carbon-coated Ni and Co nanoparticles [39]. The ratio of remnant magnetization to bulk saturation magnetization, M_r/M_s, of Co decreased from 53 to 16% and of Ni decreased from 70 to 30% as the particle diameter increased from 25 to 90 nm. It is clearly seen from this report that the smaller the particles the higher the remnant magnetization. This is due to the tendency of smaller particles to be single magnetic domains and larger particles usually contain multiple domains. The decrease in the M_r/M_s values observed in our samples may be due to an appreciable fraction of superparamagnetic particles in the samples. However, it is also possible that magnetic anisotropy may play an important role and further work is needed to achieve thorough understanding.

The coercive forces (H_c) were obtained to be 35.8, 37.6, 71.2, and 98.9 Oe for the $MgFe_2O_4$/PVP composite nanofibers calcined at 500, 600, 700, and 800 °C, respectively. These values are comparable to the values of 48.86–75.99 Oe for coprecipitation-synthesized $MgFe_2O_4$ nanoparticles (diameters of ~27.2–112 nm) [21], but are lower than the value of 165 Oe for sol–gel/combustion-synthesized $MgFe_2O_4$ (crystallite size of ~78 nm) [13]. It is seen from our results that the H_c values of the calcined $MgFe_2O_4$/PVP composite nanofibers increased with crystallite size. It is known that the variation of H_c with particle size can be explained on the basis of domain structure, critical diameter, and the anisotropy of the crystal [39–42]. Rashad [21] reported that H_c increased from 48.86 for 27.2-nm $MgFe_2O_4$ nanoparticles to 75.99 for 34.4-nm $MgFe_2O_4$ nanoparticles and then decreased to 68.11 Oe for 112-nm $MgFe_2O_4$ nanoparticles. In this case, the particle size of the 112-nm $MgFe_2O_4$ nanoparticles is possibly larger than that of the critical size and thus results in the decrease in H_c, while the particle sizes of our electrospun $MgFe_2O_4$ samples have not reached their critical size and therefore H_c was increased with increase in crystal size. The values of specific magnetization at 10 kOe, remnant magnetization (M_r), the ratio of remnant magnetization to bulk saturation magnetization (M_r/M_s), and coercive forces (H_c) are also tabulated in Table 1.

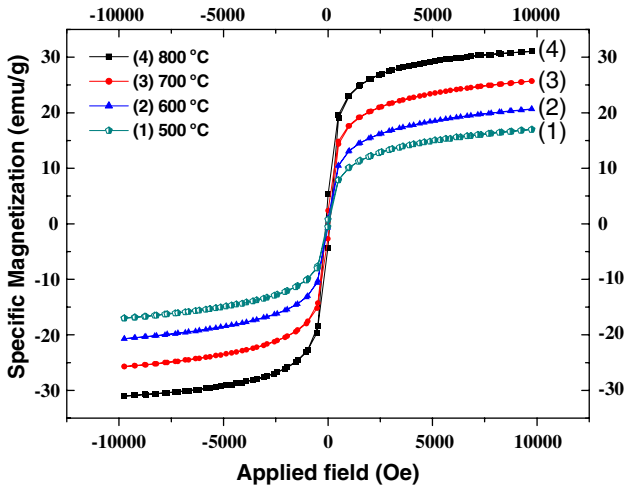

Fig. 8 The specific magnetization of the $MgFe_2O_4$/PVP composite samples calcined in air for 2 h at different temperatures, as a function of field, measured at 20 °C

Conclusion

Nanostructures of $MgFe_2O_4$ have been successfully fabricated using an electrospinning technique. Polycrystalline $MgFe_2O_4$ nanostructures (crystallite size of ~15–24 nm) as confirmed by SEAD analysis, XRD and FT-IR were formed after calcination of the as-spun $MgFe_2O_4$/PVP composite nanofibres in air at above 500 °C for 2 h. The calcined samples consisted of the structure of packed particles or crystallites of <50 nm, as revealed by SEM and TEM. The crystal structure and morphology of the calcined samples were influenced by the calcination temperature. All of the electrospun $MgFe_2O_4$ samples are ferromagnetic, having the specific magnetizations of 17.0, 20.7, 25.7, and 31.1 emu/g at 10 kOe for the samples calcined at 500, 600, 700, and 800 °C, respectively. We believe that the electrospun $MgFe_2O_4$ nanostructures could have potential in some new applications as ferromagnetic nanostructures for nanocomposites, separation, anodic material in lithium ion batteries, catalysts, and as electronic material for nanodevices and storage devices.

Acknowledgments The authors would like to thank the Department of Chemistry, Khon Kaen University for providing TG-DTA, FT-IR, and VSM facilities, the Science Lab Center, Naresuan University for providing TEM facilities, the Department of Physics, Faculty of Science, Ubon Ratchathani University for providing XRD facilities, and the Thai Microelectronics Center (TMEC) for FE-SEM facilities. This study is supported by The National Nanotechnology Center (NANOTEC), NSTDA, Ministry of Science and Technology, Thailand, through its program of Center of Excellence.

References

1. R. Valenzuela, *Magnetic Ceramics* (Cambridge University Press, Cambridge, 1994)
2. R.J. Willey, P. Noirclerc, G. Busca, Chem. Eng. Commun. **123**, 1 (1993). doi:10.1080/00986449308936161
3. S. Choi, M.H. Chung, Semin. Integr. Med. **1**, 53 (2003)
4. Z. Lai, G. Xu, Y. Zheng, Nanoscale Res. Lett. **2**, 40 (2007). doi:10.1007/s11671-006-9027-3
5. S.A. Corr, Y.P. Rakovich, Y.K. Gun'ko, Nanoscale Res. Lett. **3**, 87 (2008). doi:10.1007/s11671-008-9122-8
6. S. Wang, Y. Zhou, W. Guan, B. Ding, Nanoscale Res. Lett. **3**, 289 (2008). doi:10.1007/s11671-008-9151-3
7. W. Wu, Q. He, C. Jiang, Nanoscale Res. Lett. **3**, 397 (2008). doi:10.1007/s11671-008-9174-9

8. Z.H. Hua, R.S. Chen, C.L. Li, S.G. Yang, M. Lu, X.B. Gu, Y.W. Du, J. Alloys Compd. **427**, 199 (2007). doi:10.1016/j.jallcom.2006.02.048
9. G. Ji, S. Tang, B. Xu, B. Gu, C. Du, Chem. Phys. Lett. **379**, 484 (2003). doi:10.1016/j.cplett.2003.08.090
10. Q. Chen, A.J. Rondinone, B.C. Chakoumakos, Z.J. Zhang, J. Magn. Magn. Mater. **194**, 1 (1999). doi:10.1016/S0304-8853(98)00585-X
11. S. Verma, P.A. Joy, Y.B. Khollam, H.S. Potdar, S.B. Deshpande, Mater. Lett. **58**, 1092 (2004). doi:10.1016/j.matlet.2003.08.025
12. Y.-L. Liu, Z.-M. Liu, Y. Yang, H.-F. Yang, G.-L. Shen, R.-Q. Yu, Sens. Actuators B **107**, 600 (2005). doi:10.1016/j.snb.2004.11.026
13. Y. Huang, Y. Tang, J. Wang, Q. Chen, Mater. Chem. Phys. **97**, 394 (2006). doi:10.1016/j.matchemphys.2005.08.035
14. R.A. Candeia, M.A.F. Souza, M.I.B. Bernardi, S.C. Maestrelli, I.M.G. Santos, A.G. Souza, E. Longo, Mater. Res. Bull. **41**, 183 (2006). doi:10.1016/j.materresbull.2005.07.019
15. I. Bergman, V. Sepelak, K.B. Becker, Solid State Ionics **177**, 1865 (2006). doi:10.1016/j.ssi.2006.04.002
16. V. Sepelak, D. Baabe, D. Mienert, F.J. Litterst, K.D. Becker, Scr. Mater. **48**, 961 (2006). doi:10.1016/S1359-6462(02)00600-0
17. V. Sepelak, A. Feldhoff, P. Heitjans, F. Krumeich, D. Menzel, F.J. Litterst, D. Menzel, F.J. Litterst, I. Bergmann, K.D. Becker, Chem. Mater. **18**, 3057 (2006). doi:10.1021/cm0514894
18. V. Sepelak, I. Bergmann, D. Menzel, A. Feldhoff, P. Heitjans, F.J. Litterst, K.D. Becker, J. Magn. Magn. Mater. **316**, e764 (2007). doi:10.1016/j.jmmm.2007.03.087
19. V. Sepelak, P. Heitjans, K.D. Becker, J. Therm. Anal. Calorim. **90**, 93 (2007). doi:10.1007/s10973-007-8481-1
20. Y. Ichiyanagi, M. Kubota, S. Moritake, Y. Kanazawa, T. Yamada, T. Uehashi, J. Magn. Magn. Mater. **310**, 2378 (2007). doi:10.1016/j.jmmm.2006.10.737
21. M.M. Rashad, J. Mater. Sci. **42**, 5248 (2007). doi:10.1007/s10853-006-0389-9
22. C.-P. Lui, M.-W. Li, Z. Cui, J.-R. Huang, Y. Tian, T. Lin, W.-B. Mi, J. Mater. Sci. **42**, 6133 (2007). doi:10.1007/s10853-006-1070-z
23. D.H. Renaker, I. Chun, Nanotechnology **7**, 216 (1996). doi:10.1088/0957-4484/7/3/009
24. R. Ramaseshan, S. Sundarrjan, R. Rose, R. Ramakrishna, J. Appl. Phys. **102**, 111101 (2007). doi:10.1063/1.2815499
25. D.H. Reneker, A.L. Yarin, H. Fong, S. Koombhonge, J. Appl. Phys. **87**, 4531 (2000). doi:10.1063/1.373532
26. D. Li, T. Herricks, Y. Xia, Appl. Phys. Lett. **83**, 4586 (2003). doi:10.1063/1.1630844
27. Y.-W. Ju, J.-H. Park, H.-R. Jung, S.-J. Cho, W.-J. Lee, Mater. Sci. Eng. B **147**, 7 (2008). doi:10.1016/j.mseb.2007.10.018
28. Y.-W. Ju, J.-H. Park, H.-R. Jung, S.-J. Cho, W.-J. Lee, Compos. Sci. Technol. **68**, 1704 (2008). doi:10.1016/j.compscitech.2008.02.015
29. W. Ponhan, S. Maensiri, Solid State Sci. (2008). doi:10.1016/j.solidstatesciences.2008.06.019
30. S. Maensiri, W. Nuansing, Mater. Chem. Phys. **99**, 104 (2006). doi:10.1016/j.matchemphys.2005.10.004
31. S. Maensiri, W. Nuansing, J. Klinkaewnarong, P. Laokul, J. Khemprasit, J. Colloid Interface Sci. **297**, 578 (2006). doi:10.1016/j.jcis.2005.11.005
32. S. Naunsing, S. Ninmuang, W. Jarernboon, S. Maensiri, S. Seraphin, Mater. Sci. Eng. B **131**, 147 (2006). doi:10.1016/j.mseb.2006.04.030
33. B.D. Cullity, S.R. Stock, *Elements of X-ray Diffraction* (Prentice Hall, NJ, 2001)
34. A. Pradeep, G. Chandrasekaran, Mater. Lett. **60**, 371 (2006). doi:10.1016/j.matlet.2005.08.053
35. S. Hafner, Z. Kristallogr. **115**, 331 (1961)
36. R.D. Waldron, Phys. Rev. **99**, 1727 (1955). doi:10.1103/PhysRev.99.1727
37. G.V.S. Rao, C.N.R. Rao, J.R. Ferraro, Appl. Spectrosc. **24**, 436 (1970). doi:10.1366/000370270774371426
38. S.Y. Gregg, K.S.W. Sing, Pure Appl. Chem. **54**, 2210 (1982)
39. S. Seraphin, C. Beeli, J.-M. Bonard, J. Jiao, P.A. Stadelmann, A. Chatelain, J. Mater. Res. **14**, 2861 (1999). doi:10.1557/JMR.1999.0382
40. B.D. Cullity, *Introduction to Magnetic Materials* (Addison-Wesley Publishing Company Inc., Reading, MA, 1972)
41. S. Chikazumi, *Physics of Magnetism* (Wiley, New York, 1959)
42. M. Georgea, A. Mary John, S.S. Naira, P.A. Joy, M.R. Anantharaman, J. Magn. Magn. Mater. **302**, 190 (2006). doi:10.1016/j.jmmm.2005.08.029